Available online at www.sciencedirect.com
SCIENCE DIRECT
Tectonophysics 417 (2006) 201–220
TECTONOPHYSICS
www.elsevier.com/locate/tecto

A 3-D density–velocity model between the Cretan Sea and Libya

J. Makris [a], T. Yegorova [b,*]

[a] GeoPro GmbH, Germany
[b] Institute of Geophysics, National Academy of Sciences, 32 Pr. Palladina, Ukraine

Received 10 May 2004; accepted 1 November 2005
Available online 5 January 2006

Abstract

A 3-D density model for the Cretan and Libyan Seas and Crete was developed by gravity modelling constrained by five 2-D seismic lines. Velocity values of these cross-sections were used to obtain the initial densities using the Nafe–Drake and Birch empirical functions for the sediments, the crust and the upper mantle. The crust outside the Cretan Arc is 18 to 24 km thick, including 10 to 14 km thick sediments. The crust below central Crete at its thickest section, has values between 32 and 34 km, consisting of continental crust of the Aegean microplate, which is thickened by the subducted oceanic plate below the Cretan Arc. The oceanic lithosphere is decoupled from the continental along a NW–SE striking front between eastern Crete and the Island of Kythera south of Peloponnese. It plunges steeply below the southern Aegean Sea and is probably associated with the present volcanic activity of the southern Aegean Sea in agreement with published seismological observations of intermediate seismicity. Low density and velocity upper mantle below the Cretan Sea with $\rho \cong 3.25 \times 10^3$ kg/m^3 and V_p velocity of compressional waves around 7.7 km/s, which are also in agreement with observed high heat flow density values, point out at the mobilization of the upper mantle material here. Outside the Hellenic Arc the upper mantle density and velocity are $\rho \geq 3.32 \times 10^3$ kg/m^3 and $V_p = 8.0$ km/s, respectively. The crust below the Cretan Sea is thin continental of 15 to 20 km thickness, including 3 to 4 km of sediments. Thick accumulations of sediments, located to the SSW and SSE of Crete, are separated by a block of continental crust extended for more than 100 km south of Central Crete. These deep sedimentary basins are located on the oceanic crust backstopped by the continental crust of the Aegean microplate. The stretched continental margin of Africa, north of Cyrenaica, and the abruptly terminated continental Aegean microplate south of Crete are separated by oceanic lithosphere of only 60 to 80 km width at their closest proximity. To the east and west, the areas are floored by oceanic lithosphere, which rapidly widens towards the Herodotus Abyssal plain and the deep Ionian Basin of the central Mediterranean Sea. Crustal shortening between the continental margins of the Aegean microplate and Cyrenaica of North Africa influence the deformation of the sediments of the Mediterranean Ridge that has been divided in an internal and external zone. The continental margin of Cyrenaica extends for more than 80 km to the north of the African coast in form of a huge ramp, while that of the Aegean microplate is abruptly truncated by very steep fractures towards the Mediterranean Ridge. Changes in the deformation style of the sediments express differences of the tectonic processes that control them. That is, subduction to the northeast and crustal subsidence to the south of Crete. Strike-slip movement between Crete and Libya is required by seismological observations.
© 2005 Elsevier B.V. All rights reserved.

Keywords: East Mediterranean Ridge; 3-D density and velocity model; Bouguer and Free-Air gravity; Crustal structure; Subduction; Obduction; Accretion wedge

* Corresponding author. Fax: +49 331 288 1349.
E-mail addresses: tameg22@yahoo.com, egorova@igph.kiev.ua (T. Yegorova).

0040-1951/$ - see front matter © 2005 Elsevier B.V. All rights reserved.
doi:10.1016/j.tecto.2005.11.003

1. Introduction

Crustal shortening and subduction of oceanic lithosphere below the European continental margin and particularly beneath the Aegean microplate and the Cyprus Arc is the dominant tectonic process in the Eastern Mediterranean Sea. Several authors have, in global and regional models, estimated the relative movement of the clockwise expanding Aegean microplate relative to Africa to be 3 to 4 cm per year (McKenzie, 1978; Le Pichon and Angelier, 1979; Kastens, 1991; Jolivet et al., 1994; Le Pichon et al., 1995). This relative motion, reconstructed from geological and geophysical evidence, was recently also verified by GPS observations (Le Pichon et al., 1995; Reillinger et al., 1997; Kahle et al., 1998; McClusky et al., 2000). A simplified tectonic sketch and topography of the area is presented in Fig. 1.

As a consequence of the intense crustal shortening and subsidence due to cooling of the mantle south of Crete, sediment accumulations in the order of 10 to 14 km thickness and a submerged mountain range – the Mediterranean Ridge (MR) – were generated. This Ridge extends for nearly 1300 km, from offshore Western Peloponnese to Western Cyprus and is 150 to 300 km wide. Recent swath-mapping, sonar studies and Multi Channel Seismic (MCS) profiles (Hirschleber et al., 1994; Hartmann, 1995; Chaumillon and Mascle, 1997; Huguen et al., 2001; Fruehn et al., 2002; Polonia et al., 2002) revealed that the style of deformation permits to distinguish two structural zones, which divide the MR into an internal and an external domain. Messinian evaporites within the sediments and short wavelength surface deformations prevent deep penetration of normal incidence, high-resolution airgun signals for Multi Channel Seismic (MCS) surveys to propagate efficiently and penetrate the crust (see Chaumillon and Mascle, 1997; Fruehn et al., 2002). This technology failed to produce crustal and structural information of the deeper levels of the sediments and crust. Consequently, we have only a fairly good picture of the deformation of the upper sedimentary sequence, but not that of the crust and deeper parts of the basins (Chaumillon and Mascle, 1997; Huguen et al., 2001; Polonia et al., 2002).

The only data that has provided in-depth information for distinguishing the nature of the crust objectively are those of De Voogd et al. (1992), Truffert et al. (1993) and by Jones et al. (2002) from the reevaluation of expanding-spread seismic profiling (ESP) and 4 Ocean Bottom Seismographs (OBS) positioned on the Mediterranean Ridge. The combination of the ESP data of De Voogd et al. (1992) with Ocean Bottom Hydrophone (OBH) observations and multichannel data is another serious effort to delineate the deeper structure of the MR (Fruehn et al., 2002). The profiles they observed, however, are restricted to a very small part of this large area. Also the two-ship ESP technique used by De Voogd et al. (1992), Truffert et al. (1993) and Fruehn et al. (2002) yields one-dimensional velocity models only and is strongly limited by the assumption of lateral homogeneity along the seismic line. Still, these are the only reliable data on the crustal structure of the Mediterranean Ridge along the Hellenic Arc that have been used to constrain most of the recently published tectonic and density models.

Several new deep seismic studies have since been conducted along the external part of the Hellenic Arc between 1999 and 2001 (Bohnhoff et al., 2001; Makris and Broenner, 2001; Broenner, 2003). They have all produced new information on the crustal structure and deep sediments and permit to define the margins of the continental Aegean crust and its limits to the west and south of Crete. The location of these profiles is shown in Fig. 1b. Seismic data obtained by densely spaced OBS (60 to 70 units per profile at 3 to 4 km spacing) produced very reliable and detailed information south of and around Crete. These seismic data are used in the present study to constrain 3-D density models of the entire area between the Cretan Sea and Libya in order to better understand the regional deformation of the Mediterranean Ridge and the collision between Africa and Europe.

2. The seismic data and the empirically derived density values used in constraining the 3-D models

In Fig. 2 we present five seismic cross-sections that were used to constrain the density models. At the northern part, thin continental crust (15 km at its thinnest) floors the Cretan Sea (Makris, 1977, 1978; Hartung, 1987; Bohnhoff et al., 2001). As it is seen in profile 4 (Fig. 2d), the crust thickens to 32 km below Crete and is at the western part of the island in contact with the oceanic lithosphere, which is decoupled from the continental crust at the eastern part of Crete, building a subduction slab below the southeastern Aegean Sea (Bohnhoff et al., 2001). South of Crete, the continental crust thins significantly again to 18 km thickness (Bohnhoff et al., 2001; Makris and Broenner, 2001; Broenner, 2003). The seismic data indicate that continental crust extends between 60 and 100 km south of Crete before its abrupt termination and tran-

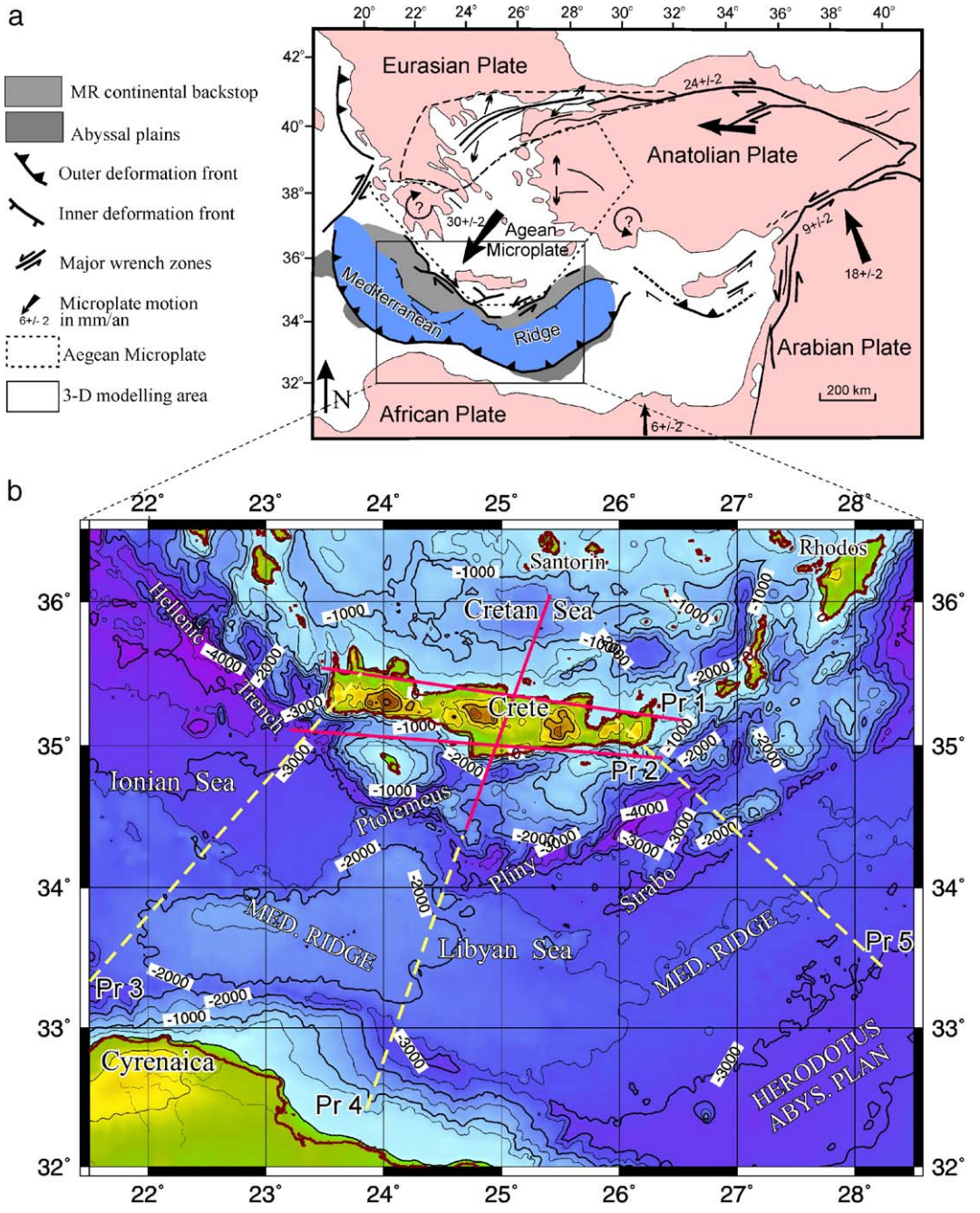

Fig. 1. (a) Tectonic context and general kinematics in the Eastern Mediterranean (from McClusky et al., 2000; Chaumillon et al., 1996; Le Pichon et al., 1995). Main microplate boundaries are shown, as well as the Hellenic trough system and the Mediterranean Ridge outer and inner fronts of deformation. Arrows with numeric values indicate regional motions. (b) Bathymetry map of the Eastern Mediterranean Ridge where the 3-D gravity modelling (rectangle in (a)) was undertaken. Lines show the position of seismic cross-sections in the Crete area (red lines, Bohnhoff et al., 2001) and in the Libyan Sea crossing the Mediterranean Ridge (yellow dashed lines, Makris and Broenner, 2001; Broenner, 2003).

sition to the oceanic crust of the Libyan Sea. This continental edge is the backstop of thick sediments that have been accumulated on the oceanic lithosphere due to the cooling and sagging of the oceanic lithosphere of the Ionian and Libyan Seas and their thickening and deformation due to subduction below the Aegean microplate. Lateral changes of the physical parameters at this border are most spectacular since the thickness of the sediments and crust, their velocity, density and accumulation of stresses through deforma-

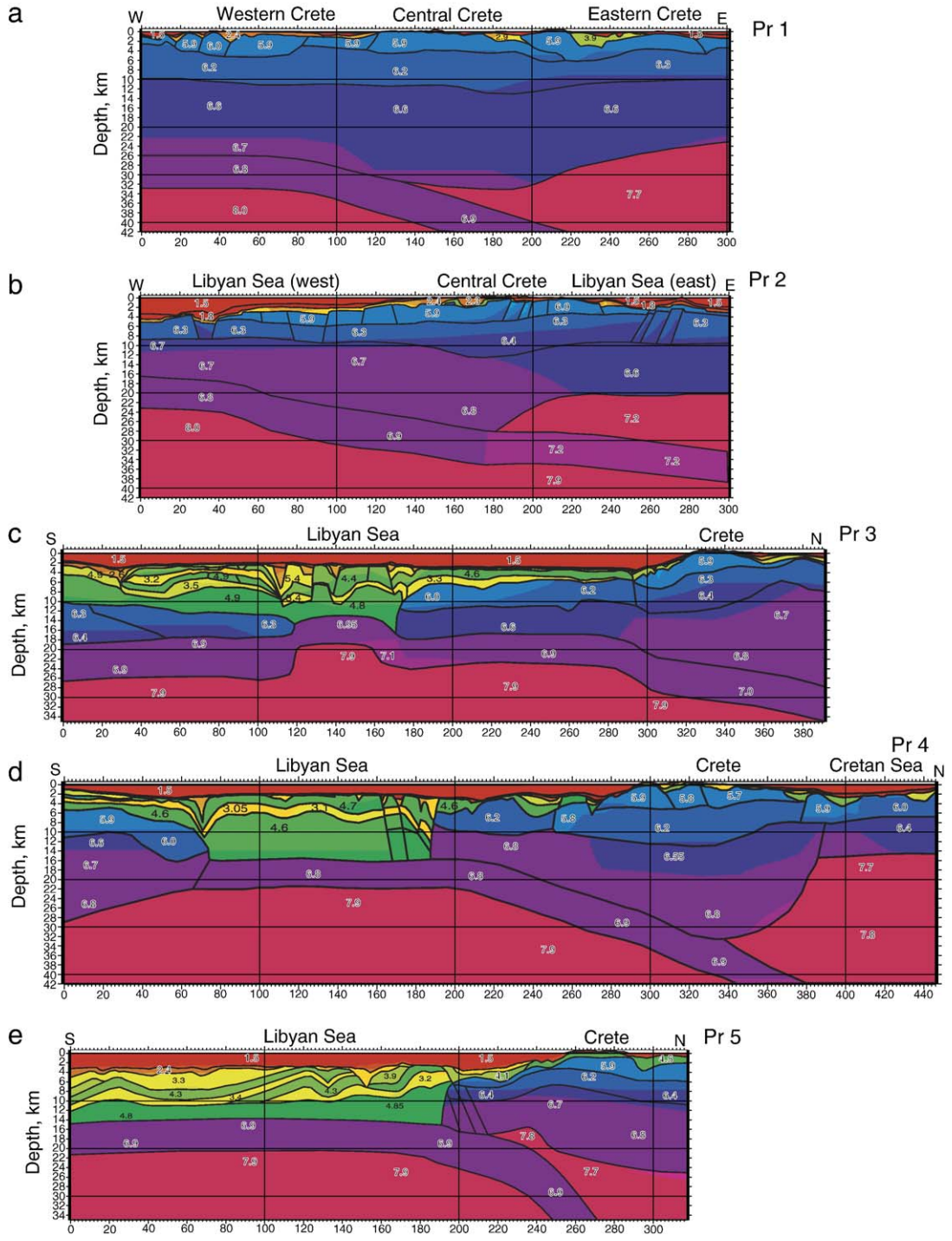

Fig. 2. Velocity cross-sections for the crust and uppermost mantle of the East Mediterranean Ridge (for the location see Fig. 1b) used in present 3-D gravity modelling. Profiles Pr 1, Pr 2 and the northern part of Pr 4 cross the area of Crete (Bohnhoff et al., 2001), profiles Pr 3, southern part of Pr 4 and Pr 5 (Makris and Broenner, 2001; Broenner, 2003) cross the Mediterranean Ridge. Numerical values indicate the V_p velocities in kilometers per second.

Table 1
Initial density values used in the 3-D modelling of the area south of Crete

Layer	V_p, km s^{-1}	ρ, 10^3 kg/m^3
Light sediments	>3.5–4.0	2.3
Compacted sediments	4.5–5.9	2.6
Continental upper crust	6.0–6.4	2.75
Continental lower crust	6.5–6.7	2.85–2.90
Oceanic crust	6.8–7.0	2.90–3.02
Normal upper mantle	8.0	3.3
Anomalous upper mantle	7.7	3.22

Velocity values were taken from the seismic profiles shown in Fig. 2.

tion are dramatic when crossing from the Aegean continental to the oceanic domain of the Libyan and Ionian Seas.

With a thickness of more than 14 km, the sediments are compressed and underthrusted below the stretched Aegean continental lithosphere and most probably dragged along with the oceanic lithosphere into the subduction zone below western Crete and the southern Aegean Sea. The transition of the oceanic crust to the African continental margin at the southern end of the seismic profiles was encountered 60 km north of the coast of Cyrenaica (profile 4, see Fig. 2d). The sediments thin from 14 km in the oceanic domain to between 4 to 6 km on the continental shelf. The continental crust thickens rapidly to between 22 and 24 km offshore Cyrenaica. The P_n velocity of the compressional waves in the upper mantle was not directly obtained for all seismic lines. In most cases PmP reflections from the crust–mantle boundary were used to define crustal thickness. The V_p velocities in the upper mantle were partly estimated from the seismic impedance contrast at the crust–mantle transition. From amplitude modelling using the observed PmP reflections and some direct observations the P_n velocity of 8.0 km/s (Broenner, 2003) was determined south of Crete, while north of it the V_p velocities of P_n-phases velocity are 7.7–7.8 km/s (Makris, 1977, 1978; Hartung, 1987; Bohnhoff et al., 2001).

The density values used in the 2-D and 3-D gravity modelling were constrained by the velocity observations (see Table 1 above and Fig. 3) and estimated from the Nafe–Drake (Nafe and Drake, 1963) and the Birch empirical functions between V_p and density (Birch, 1960, 1961). A 2-D density model along profile 3 (for the location see Fig. 1b) is presented in Fig. 4 as an example of the 2-D modelling performed at the initial stage in order to establish the geometry of the initial density model. The parameters used are presented in Table 1.

3. The gravity data: Bouguer and Free-Air anomalies

The gravity data used in the density modelling have been presented in several publications (Makris, 1977; Morelli et al., 1965; Makris et al., 1998). The data were collected during the regional surveys by the Osservatorio Geofisico Sperimentale—OGS (Morelli et al., 1965), of the University of Cambridge (Department of Geodesy and Geophysics, Cambridge University, 1975) and by the Institute of Geophysics University of Hamburg (Hartung, 1987). The technique and instrumentation used have been discussed in the above referred publications. Here we present a brief review of the accuracy and reliability of these data, since these affect the accuracy of the results obtained by the 3-D gravity modelling.

OGS (Triest) and the University of Cambridge, using Askania GKSS-2 type gravity meters and Decca radio navigation, collected marine gravity data during a regional survey of the Mediterranean Sea in the 1960s and early 1970s (Makris and Morelli, 1994; Makris et al., 1998). The resulting accuracy and resolution of the marine gravity data are not better than ±3 to 4 mGal.

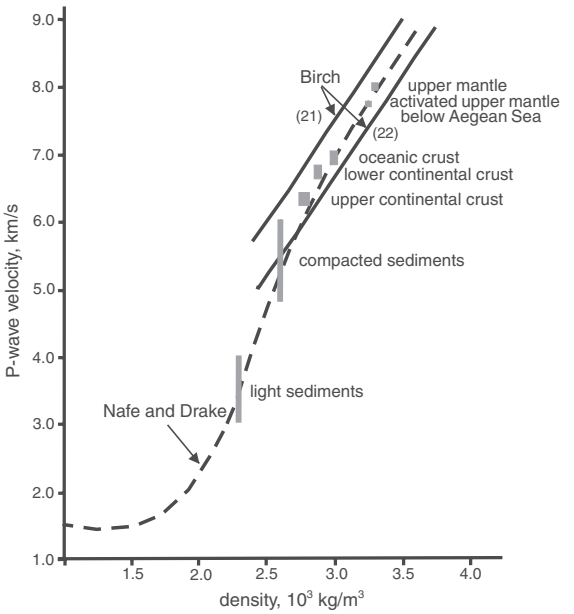

Fig. 3. Diagram of the density/velocity relation for the sediments, crystalline crust and uppermost mantle (shown also in Table 1) for the Eastern Mediterranean Ridge area, used for the gravity modelling. The velocity values were taken from the seismic observations along five profiles shown in Fig. 2. The density values were constrained by these velocity observations (Fig. 2) and estimated from Nafe–Drake (dashed line) and Birch (solid lines, shown for atomic mass 21 and 22) conversion functions.

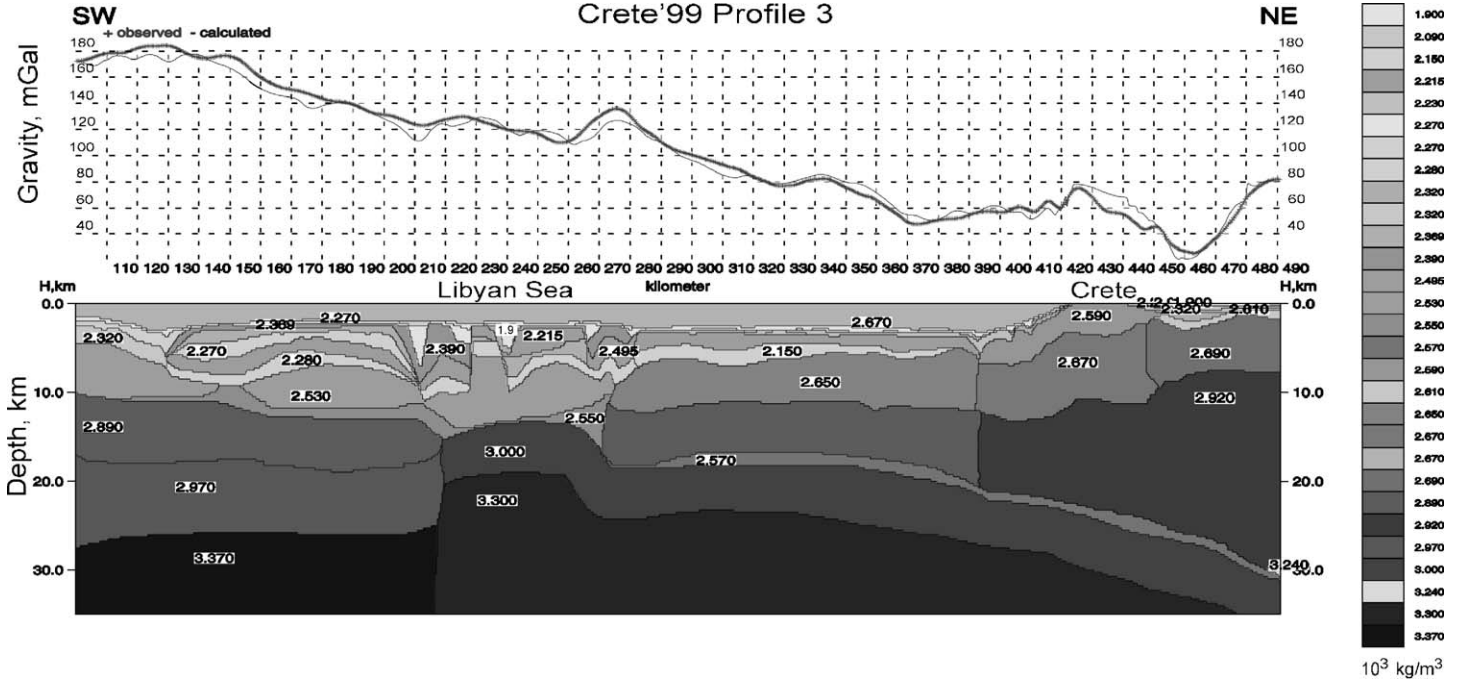

Fig. 4. Initial density model along Profile 3. Numerical values indicate densities in $\times 10^3$ kg/m^3 derived from velocities of the section Pr 3 in Fig. 2 using the empirical velocity/density function shown in Fig. 3.

This is due to the fact that the Askania GKSS-2 system is a horizontal pendulum and therefore affected by cross-coupling effects depending on weather. The large period T of the system does not allow to record rapid gravity changes and filters high frequency effects. The second problem is that of navigation accuracy and the velocity values defined for the moving ship used in computing the Eötvös-effect. As discussed by Morelli et al. (1965), Makris and Morelli (1994) and Makris et al. (1998), navigation and, consequently, the ship speed, as well as the wide spacing of the ship tracks (10 km between profiles) in the Eastern Mediterranean Sea had a negative influence on the accuracy and resolution obtained during these surveys. Only recently and after the extensive use of a linear gravity meter of the Askania new generation, known as the BodenSee gravimeter type KSS-30/31, and GPS-navigation, the accuracy of the gravity surveys can be improved up to ±0.5 to 1.0 mGal. Therefore now, the resolution of the field intensity therefore depends on the spacing of the ship tracks. For the area of Aegean Sea, the Cretan Sea in particular, and also directly to the south of Crete, we spaced our profiles at 1.5 to 3 km. A comparison of old data with new ones shows that even in the areas of steep gradients the gravity anomalies are in agreement within ±5 mGal. We therefore modelled the anomalies to a degree of coincidence between observed and calculated gravity that was not necessarily better than ±3 to 5 mGal. In areas of large spacing of the gravity profiles and far from the location of the available seismic lines, we considered only the regional field and did not attempt to explain its high frequency components. For areas not covered by shipborn data of OGS (Morelli et al., 1965) and the University of Hamburg (Hartung, 1987), we used 2′ gridded satellite data (available at http://topex.ucsd.edu) and partly those published by Sandwell and Smith (1997), which continued downwards to the sea surface. The data of the satellite observations are reliable outside the coastal region of Crete and for this reason we densed the marine data directly offshore south Crete in 1999 by a survey with the RV-Aegeo using the Bodenswerk KSS-30 gravity meter of the University of Hamburg. The satellite observations published by Raytheon Company, USA (available at http://magus.stx.com, responsible Y.M. Wang; see also Chapin, 1998) are reliable in the lower spectrum of the field and sufficient for regional modelling. In this way we improved the quality of the gravity information, increasing the field resolution in areas not covered by marine data.

Modelling in 2- and 3-D was based on the Bouguer gravity field, in order to have a better comparison between the onshore with the offshore anomalies. In addition, the reliable and exact bathymetry presented by Morelli and Val'chuk (1988) allows an exact calculation of the Bouguer effect and Bouguer anomalies. The Bouguer map (Fig. 5) shows positive Bouguer values of +160 mGal in the Cretan Sea where the continental crust is thin and the sediments do not exceed 3000 m in thickness. The Cretan Arc is clearly formed by a series of gravity anomalies that range between +40 and +20 mGal and follow the arc from south Peloponnese, Crete, and Carpathos to Rhodos and present a regional, arcuate gravity low due to the increase of the crustal thickness. As previously stated, a maximum of 32 km thick continental crust was located below central Crete (Makris, 1977; Makris and Stobbe, 1984; Bohnhoff et al., 2001). In front of the Cretan Arc we have intense variations of the gravity anomalies and their gradients. It is also obvious from the velocity models that lateral density changes will be intense between the Aegean Sea and the Hellenic Arc or the deep-sea areas. The largest positive Bouguer anomaly (up to +180 mGal) is observed just northeast of Cyrenaica and offshore northwest Egypt (see also Makris and Wang, 1994). It is obvious that the gravity observations without well-constrained initial density models by seismic data cannot be used to produce density models of any degree of reliability or uniqueness. The isostatic balance is by no means established in all areas (Makris, 1977) and the deformation of the geoid between Greece and the Ionian and the Cretan Seas has one of the largest local anomalies worldwide (Brennecker et al., 1983).

The Free-Air (FA) anomaly map presented in Fig. 6 was not used for modelling. It shows interesting gravity features and strongly reflects the morphological and density contrasts between the elevated Aegean crust and topography and the deep depression in the Hellenic Trench (deepest part of the Mediterranean Sea with over 5000-m depth). The Hellenic Trench coincides with the strongest negative FA anomaly of −200 mGal. Also the Ptolemeus, Pliny and Strabo trenches have strong gravity expressions in Fig. 6 that coincide with abrupt morphological changes. It seems that in this area normal faulting due to extension dominates the present deformation. Strike-slip movements of NE–SW orientation were reported by McKenzie (1978) and Huguen et al. (2001) and were confirmed by focal mechanisms published by Pondrelli et al. (2002) showing sinistral strike-slip movements south of Crete.

The Rhodes Abyssal plain located to the SE of Rhodes is equally interesting and little understood area. Unfortunately, we have no seismic information in this area and it is difficult to explain the development

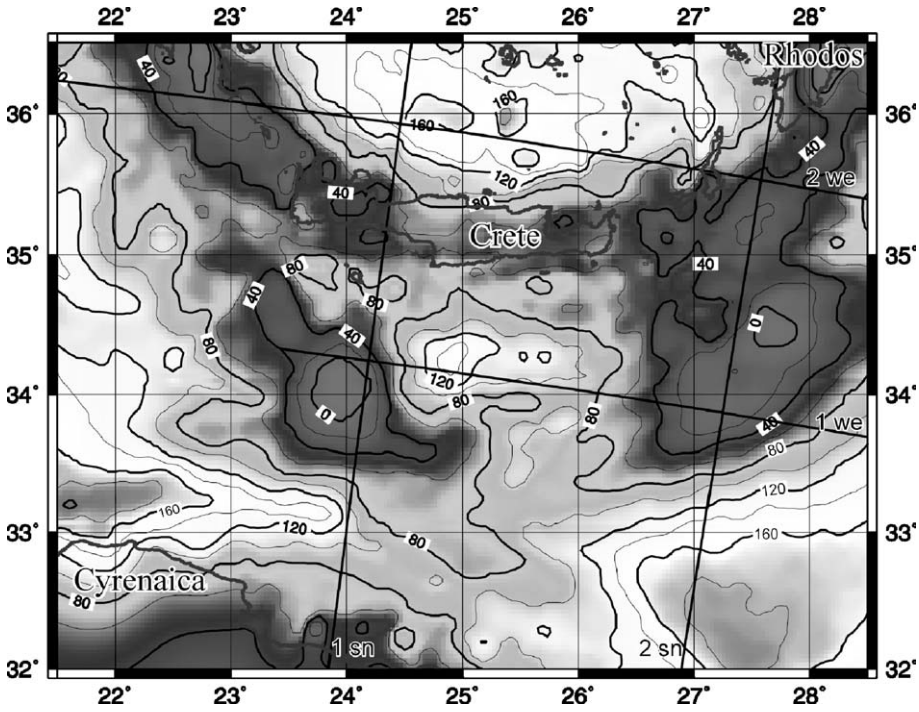

Fig. 5. Observed gravity field (Bouguer anomalies) used in 3-D gravity modelling for the Eastern Mediterranean Ridge between Crete and Libya. Contour interval is 20 mGal. Lines (1 sn, 2 sn, 1 we and 2 we) indicate the position of orthogonal cross-sections (shown in Figs. 9 and 10) of the 3-D gravity model.

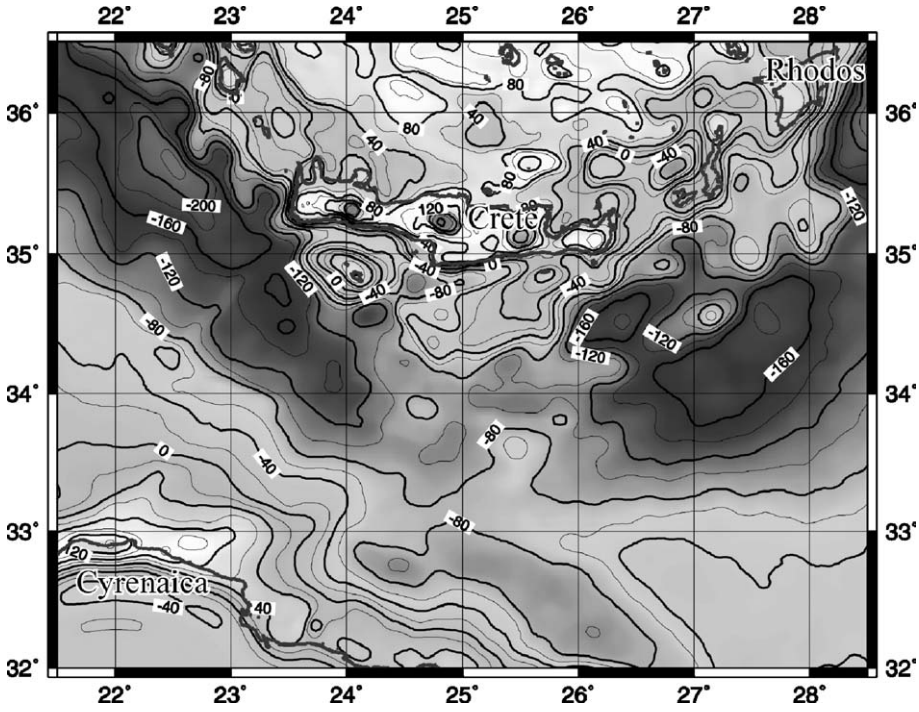

Fig. 6. Free-Air gravity anomalies for the Eastern Mediterranean Ridge between Crete and Libya. Contour interval is 20 mGal.

of the escarpment between Rhodes and the Rhodes abyssal plain with an elevation difference of more than 2000 m. Crustal thickness and crustal type are unknown for this area.

4. Gravity modelling procedures

In order to develop the initial 3-D density models we used the seismic results and computed 2-D density models along the seismic lines using the Talwani et al. (1959) algorithm. An example is presented in Fig. 4. The software has been completely modified by Tchernychev (personal communication) for the 2-D and by Tchernychev and Makris (1996) for the 3-D case. This new program, GRAVMAG, can be used for both 3-D gravity and magnetic modelling. It is interactive and very fast. This approach permits to model large areas of very complex structure in a moderate time. Results after model modification are obtained in real time. Details of the computational approach are presented in the mentioned cited works. In brief, the 2-D and 3-D bodies are approximated by prisms defining areas of constant density. The prism size used in this study is $4\times4\times0.5$ km^3. The geometry of a given body is discretized by elementary prisms of constant size and the gravity effect of this prism is computed for density 1×10^3 kg/m^3 as a function of distance. The gravity effect of a body for a given point at the surface is obtained by computing the distance of each prism to the point on the surface and by summing the gravity effects of all prisms after they have been multiplied by their density values:

$$\delta g_i = f\left(\delta g_{pr}/r_i\right), \quad \Delta g_B = \rho_i \sum \delta g_i \qquad \text{where}$$

δg_{pr} is the gravity effect of the elementary prism and r_i are its coordinates in a Cartesian system, Δg_B—the gravity effect of the complete body obtained by summing the gravity effects of the prisms included in an area and multiplied by the appropriate densities.

The initial model is defined by surfaces extrapolated from 2-D models computed along the seismic lines (Fig. 2). This model is improved by 2-D gravity modelling of a few additional profiles interpolated in between the original density models along the seismic lines. Thus we avoid systematic or excessive errors in defining the initial 3-D geometry of the space we want to model and optimize the 3-D modelling time by limiting the iterations needed to fit the calculated to the observed anomalies.

Modifications of the 3-D model are obtained interactively using the "digging method" (Tchernychev and Makris, 1996). Any part of the model can be redefined by projecting its cross-section on the computer screen and then introducing the required changes interactively. Changes perpendicular to the cross-section exposed on the screen are defined by stating for how many prisms perpendicular to the exposed cross-section the introduced modification must apply. This permits a convenient and fast model change since the 2-D visualization of a 3-D volume is accomplished very rapidly.

GRAVMAG uses relative densities or density excess for gravity calculations. That means that some value for a reference density should be set as a parameter. The program uses average density parameter–a constant value representing the average density for an 'average' column of the model from surface to base of the model, which contains different geological layers–from sea water down to the upper mantle (from zero down to 50 km). In our case the average density for 3-D calculations was adopted as 3.0×10^3 kg/m^3. The side effect is taken into account from the bodies which are supposed to be non-local (an expression for the field from a rectangular shape is used), their gravity effect with the average density is calculated (from the infinite plain for a layer) and summed for the whole model. GRAVMAG operates on flat model; therefore data presented in geographical coordinates should be projected on the plan. Our maps presented in Mercator projection were projected into local system using the GMT package (Wessel and Smith, 1998).

The following surfaces were constructed by interpolation and used for the initial model: (1) bathymetry map (sea bottom that defines also the top of light sediments); (2) top of dense compacted sediments (base of light sediments); (3) top of the continental upper crust; (4) top of the continental lower crust; (5) top of the oceanic crust; (6) base of the continental crust —Moho$_c$; and (7) base of the oceanic crust—Moho$_o$.

The initial densities for the layers, confined by the above described surfaces, are presented in Table 1.

In Fig. 4 we presented an example of the initial density model along a seismic 2-D cross-section profile 3 (Fig. 2c). In order to reduce the computational effort and since our main interest rests with the regional behavior of the structures, we simplified the complexity of the sediments and divided the sedimentary successions into two layers: an upper one having an average density ($\bar{\rho}$) of 2.30×10^3 kg/m^3 and a deeper one with $\bar{\rho}=2.60\times10^3$ kg/m^3. The overall thickness of the sedimentary sequence derived from the seismic model was taken as a fixed parameter. In doing so we neglected sediments with a small velocity inversion located south of Crete. As we will show later, this produced a local systematic discrepancy between observed and comput-

ed gravity in the order of 10 mGal. This is of no significance for the regional discussion, the crustal thickness and its nature or tectonic implications derived from the 3-D density model.

A peculiar feature of the sedimentary successions of the MR is the presence of Messinian evaporates, served as a décollement level for the formation of the MR accretionary wedge and which can influence the gravity modelling results. In the western part of the MR the evaporates are as much as 2 km thick, and beneath the Herodotus abyssal plain, in front of the eastern part of the MR, the thickness of evaporates reach 4 km (De Voogd et al., 1992; Truffert et al., 1993; Fruehn et al., 2002; Reston et al., 2002; Jones et al., 2002). In our gravity modelling the evaporates, having velocities 4.0–4.5 km/s and density 2.2×10^3 kg/m^3 (De Voogd et al., 1992; Truffert et al., 1993; Chaumillon and Mascle, 1997; Huguen et al., 2001; Polonia et al., 2002), are not explicitly included in the model as a separate layer, since they do not constitute a continuous layer over the entire study region. However, they are mostly included in the upper layer of light sediments with $\rho = 2.3 \times 10^3$ kg/m^3, which are buried down to 8–10 km depth in the MR. Thus we avoid systematic errors due to presence of evaporates when calculating the gravity effect of sediments.

5. Results of the 3-D modelling

By applying the computational procedure described above we developed a 3-D density model extending from 21.5° to 28.5° E and 32.0° to 36.5° N. It covers in the north the area of the Cretan Sea and extends to the south to Cyrenaica and the coast of Egypt. At depth the model was limited to 50 km. The space involved in the 3-D computations is contained in a volume of 700 km EW × 520 km NS × 50 km in the vertical. The elementary prism used to discretize the model is $4.0 \times 4.0 \times 0.5$ km^3. The results are represented by the maps for the sediments overlying the basement – continental and oceanic (Fig. 7) – and the Moho (Fig. 8), which also contains continental and oceanic parts. In Fig. 9 we present two NS-oriented cross-sections and in Fig. 10—two of WE-oriented cross-sections, respectively. The synthetic gravity map that resulted from the 3-D calculations is shown in Fig. 11 and the gravity residuals, obtained by subtracting the computed gravity from the observed one, are given in Fig. 12.

We developed a smoothed, regional density model and omitted the interpretation of local anomalies. The additional computation effort needed to adjust all details of the high frequency part of the field is not justified by the accuracy of the gravity data or by spacing of the seismic lines. The synthetic gravity field (Fig. 11) when compared to that observed (Fig. 5) shows that all broad features of the maps are to a great extent identical. The residual anomalies shown in Fig. 12 are for most parts of the map within ± 5 mGal. Only along the Hellenic Trench west of Peloponnese and to the southeast of Crete, the residual values are in the order of − 20 mGal. Considering the fact that the maximum Bouguer gravity amplitudes range between 140 to 180 mGal, filtering the high frequency components causes a maximum discrepancy between observed and computed field in the order of ± 12% to 14%. We considered this as not significant and without any consequence for the regional discussion. Another justification can be obtained from the visual inspection of the matching of observed and calculated fields along the four 2-D profiles presented in Figs. 9 and 10. In all these models the amplitudes of the gravity anomalies and the gradients of the field are satisfied within 5%.

From the NS density models shown in Figs. 4 and 9 we see several characteristics common in all three of them. The African continental crust extends up to 100 km offshore north of Cyrenaica and its thickness is 29 to 25 km before its transition to the oceanic crust of the Libyan Sea. The sediments on the African continental shelf thicken seawards to more than 8 to 10 km. The truncation of the African continental crust and that of the sediments towards the oceanic domain at the MR is very abrupt. The MR further north is characterized by intense deformation of sediments accumulated on an oceanic crust of more than 13 km in thickness (Figs. 7 and 9). This significant subsidence occurred mainly by cooling and sagging of the oceanic lithosphere, but also due to crustal shortening and accumulation of sediments in an accretionary wedge. Heat flow density values published by Cermak et al. (1977) and the distribution of the isotherms (Makris and Stobbe, 1984) support the concept of subsidence due to cooling as the major driving force for the development of the deep basins. Accretion is mainly developed to the west and the northwest of the Aegean margin and Crete (see e.g. Truffert et al., 1993; Fruehn et al., 2002) due to the northeast orientation of subduction of the oceanic crust (see Fig. 4), which is in agreement with previous seismic studies, seismic tomography and gravity modelling (Polonia et al., 2002; Spakman et al., 1988; Papazachos and Nolet, 1997; Tsokas and Hansen, 1997). The Aegean crust south of Crete is covered by much thinner sediments, starting with 6 to 7 km thickness immediately at the edge of the margin and thinning gradually towards

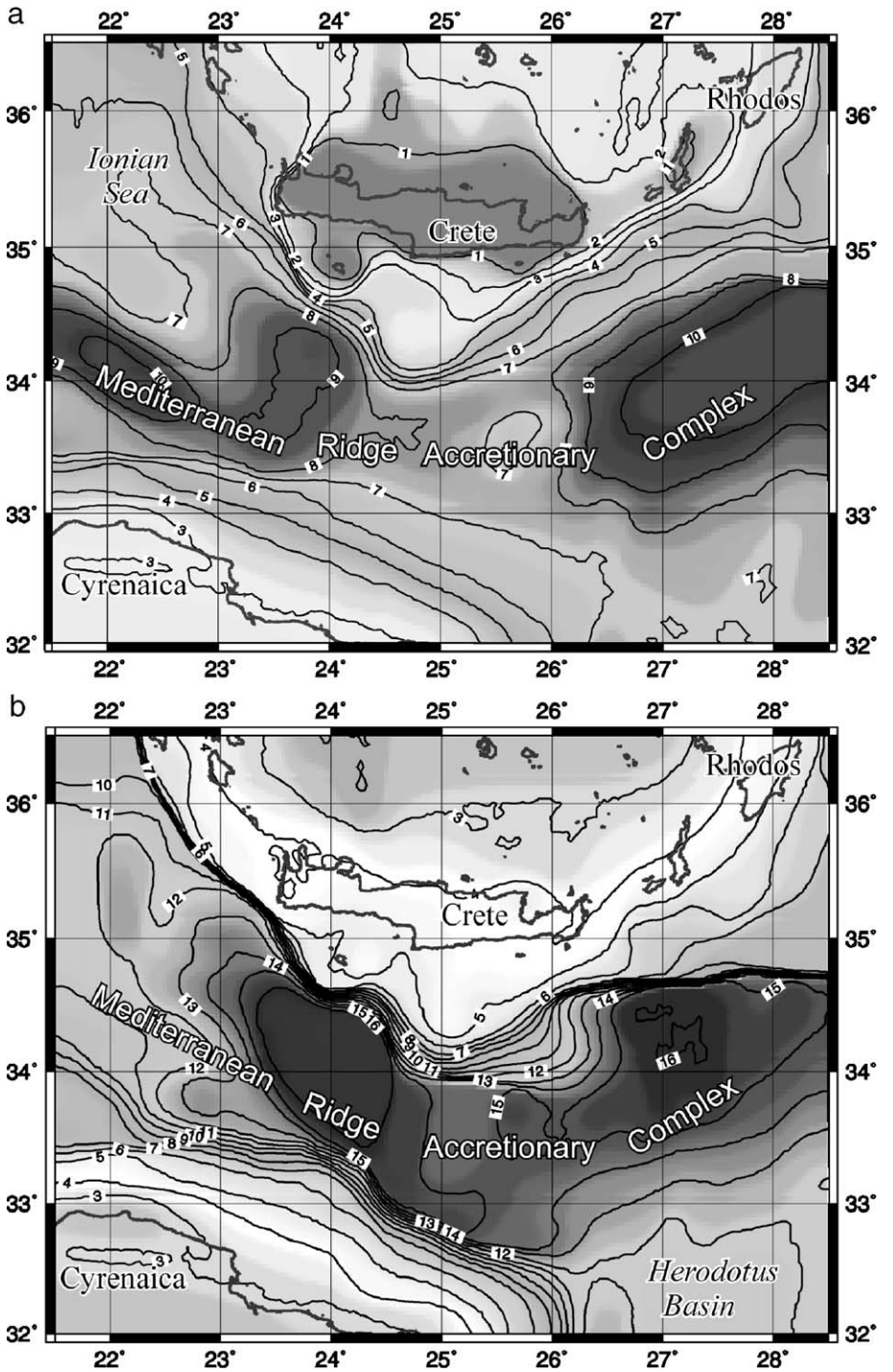

Fig. 7. Depth (km) to the bottom of sediments — light, $\bar{\rho}$ $=2.3\times10^3$ kg/m^3 (a) and compacted, $\bar{\rho}$ $=2.6\times10^3$ kg/m^3 (b), derived as a result of 3-D gravity modelling for the Eastern Mediterranean Ridge. The bottom of sediments (b) (top of crystalline continental and oceanic crust) is also shown in Fig. 13 in a 3-D view.

Crete to 4 km. A layer with significant velocity/density inversion shown in Fig. 4 is located below the limestone (2.2 to 2.3×10^3 kg/m^3) and is terminated onshore Crete where a highly metamorphic limestone (Plattenkalk series) of 2.58×10^3 kg/m^3 density is exposed. The crust below the sediments at the Libyan

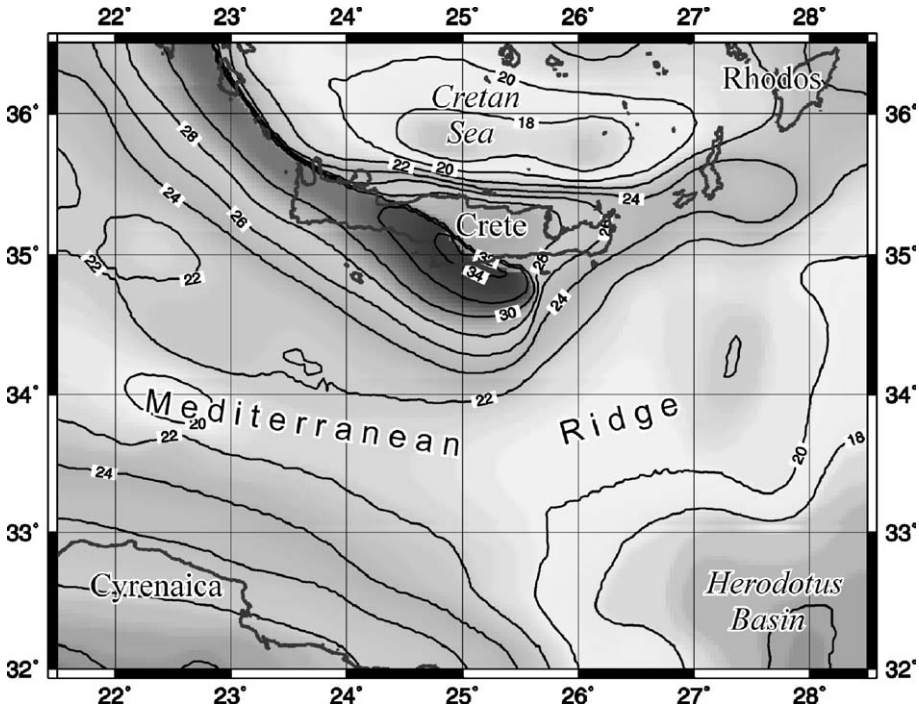

Fig. 8. Depth (km) to the top of the upper mantle (base of continental and oceanic crust) derived from 3-D gravity modelling for the Eastern Mediterranean Ridge between Crete and Libya. It is also shown in Fig. 14 in a 3-D view. The crust thickening (to 34 km) is distinguished along the NW–SE subduction front beneath southern Peloponnese, western Crete and to the south of central Crete where oceanic crust of Libyan and Ionian Seas meets the continental Aegean crust.

margin is about 17 km thick, while the oceanic one below the MR is only 6.5 km. The Aegean continental margin south of Crete was found to be composed of 10 km continental plus 6.5 km of subducted oceanic crust. The total thickness is 16.5 km and the sediments on top, 6 to 7 km. Below western Crete we have a crust of 21 to 25 km of continental origin followed by 6.5 km of oceanic crust. If we consider the 3 to 4 km of metamorphic limestone at the top of this crust, we find the Moho below the western Crete at 30 to 32 km depth, as defined by Makris (1977), Makris and Vees (1977), Tsokas and Hansen (1997) and Bohnhoff et al. (2001) from seismic profiles along Crete in EW direction.

The last observation that becomes obvious when considering these density models is the density decrease in the upper mantle from the African–Mediterranean to the Aegean domain. From 3.32×10^3 kg/m^3 density below Libya, we have 3.3×10^3 kg/m^3 below the MR and only 3.25×10^3 kg/m^3 below the Cretan Sea. Makris (1977), Makris and Stobbe (1984) and Bohnhoff et al. (2002) came to the same conclusion. After subtracting the gravity effect of the crust/sediments from the observed field, the remaining gravity residuals reach 40 to 50 mGal below the southern Aegean Sea. This can only be compensated by decreasing the upper mantle density below the Cretan Sea.

The WE lines shown in Fig. 10 confirm what was described from the 3 NS lines. The arcuate belt along the southern Peloponnese, Crete and Rhodes is distinguished by a relative gravity low due to crustal thickening. The gravity high in the Cretan Sea is explained by the lack of sediments, intense thinning of the crust and updoming of the mantle. Lateral changes of the mantle density (see Fig. 10b) are required in order to model the regional gravity field. In this regard the Ionian mantle should be of higher density than that of the Cretan Sea (see also Makris, 1977; Makris and Stobbe, 1984; Tsokas and Hansen, 1997; Casten and Snopek (2006)).

Profile 1 WE in Fig 10a is located at the MR outside the Hellenic Arc crossing the Libyan Sea from southwest of Crete to southeast of Crete. The two gravity lows in this area, seen in Fig. 5 with values of 40 to 0 mGal, which are separated by a gravity high of 120 mGal, define two depositional centres of great accumulation of sediments in the MR. These two areas of large thickness of sediments over oceanic basement are separated by thinned continental crust extending south of Crete for nearly 100 km off the

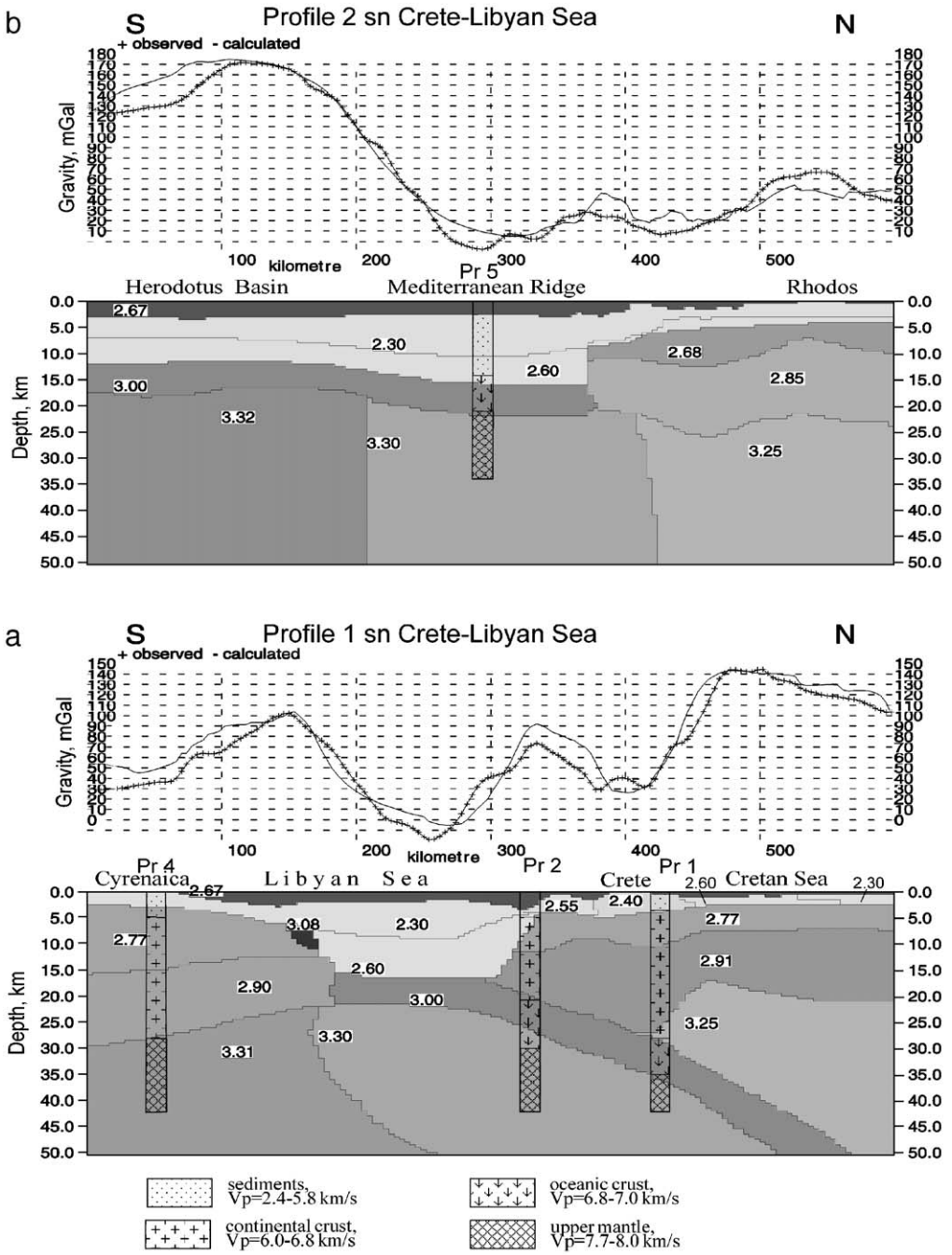

Fig. 9. Two NS-oriented density cross-sections inferred by 3-D gravity modelling of the Eastern Mediterranean Ridge between Crete and Libya (for the location see Fig. 5) and observed and computed Bouguer field. Numeric values show the density (10^3 kg/m^3) derived from Fig. 3 and Table 1. Vertical columns show the velocity structure of the seismic profiles (Fig. 2), where they intersect the density cross-sections.

Cretan coast. This is better demonstrated by considering in Fig. 7 the map of sediment thickness south of Crete. The sedimentary basins south of the western end and eastern parts of Crete with more than 13 km in thickness are separated by an uplifted block with thinner sediments, high gravity values of 120 mGal, and, as seen in Fig. 10, floored by continental "Aegean" crust, while that below the deep sedimentary basins is of oceanic origin. It is obvious that the indentation of the boundaries between the continental and oceanic crustal areas between Europe and Africa is more complex than assumed before, e.g. by Huguen et al. (2001),

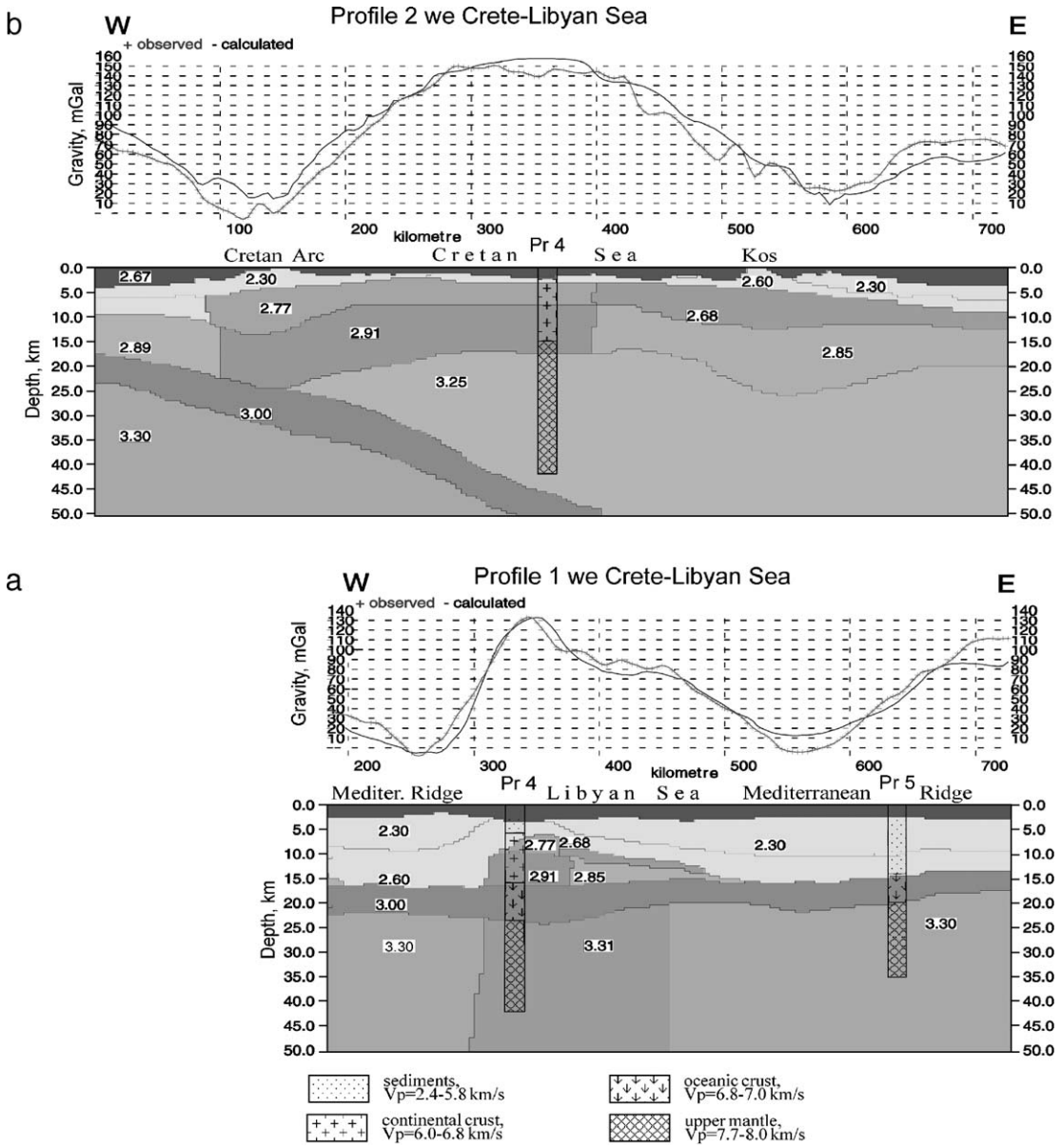

Fig. 10. Two WE-oriented density cross-sections inferred by 3-D gravity modelling of the Eastern Mediterranean Ridge between Crete and Libya (for the location see Fig. 5) and observed and computed Bouguer field. Numeric values show the density (10^3 kg/m^3) derived from Fig. 3 and Table 1. Vertical columns show the velocity structure of the seismic profiles (Fig. 2), where they intersect the density cross-sections.

Makris and Broenner (2001) and Broenner (2003), expressing changes in orientation of the differential movement between the two margins in time.

Fig. 13 represents a 3-D view from southeast to northwest of the basement top (bottom of sediments (see map in Fig. 7b)). The continent–ocean transition between the deep oceanic basin over the MR and the uplifted continental edge south of Crete are clearly seen. The widened oceanic crust towards the Herodotus area of the Eastern Mediterranean Sea narrows to the northwest to nearly 60 km before its opening to the Ionian oceanic domain, where it widens again. This is also seen in two N–S sections in Fig. 9. The 3-D model in Fig. 13 shows the location of the closest proximity between continental Africa and continental Europe just before the initiation of the continent–continent collision. From this picture it is also obvious that the complexity of the backstop limit of the accretion wedge

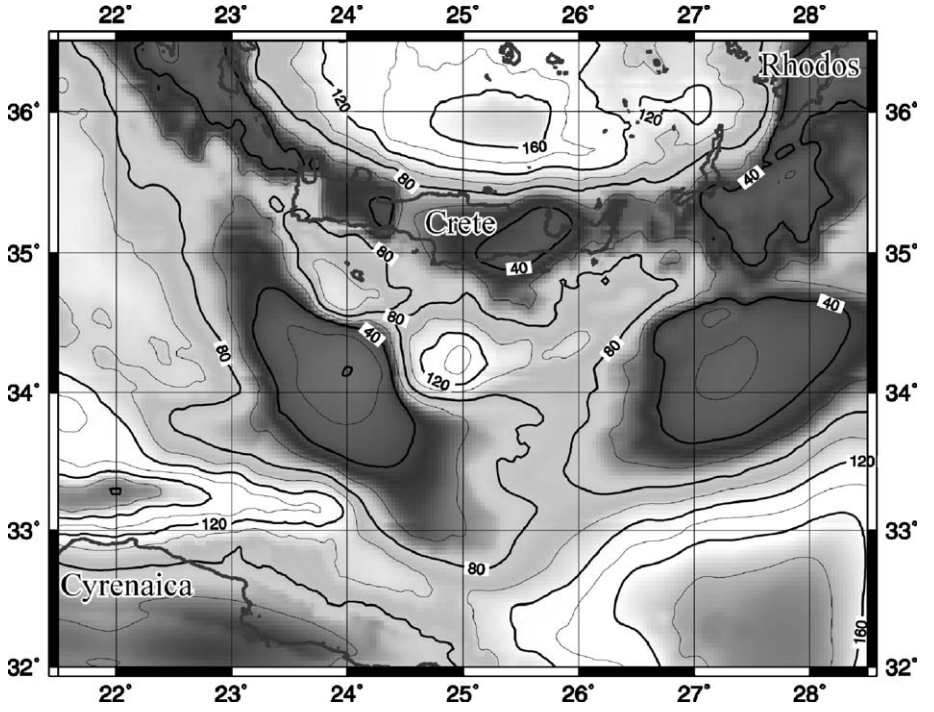

Fig. 11. Calculated gravity effect of the 3-D gravity model of the Eastern Mediterranean Ridge between Crete and Libya. Contour interval is 20 mGal.

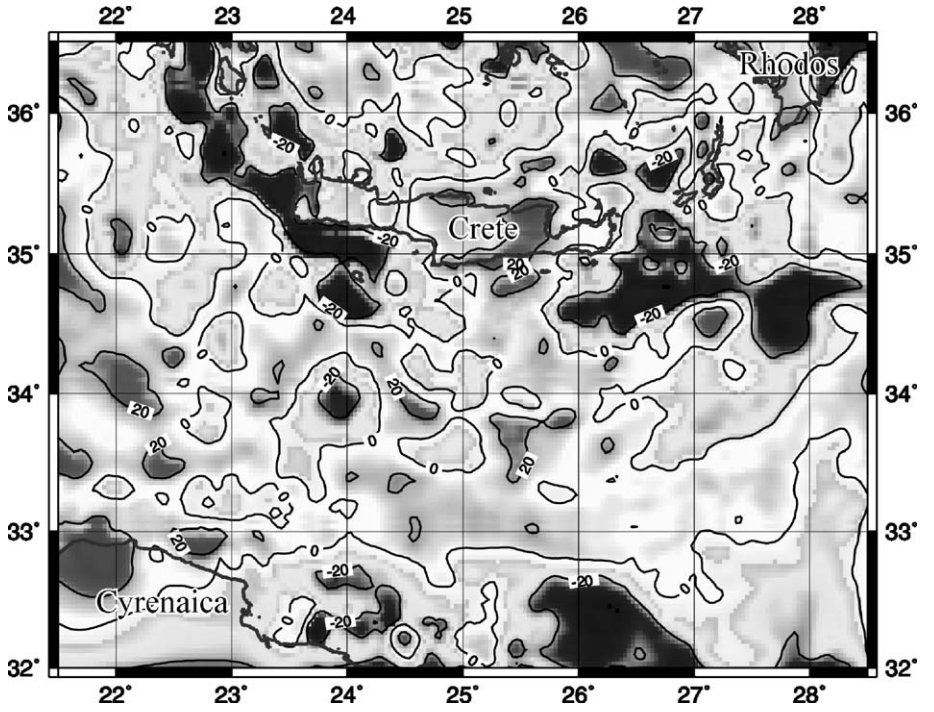

Fig. 12. Residual gravity field of the study area obtained by subtracting the calculated gravity effect of the 3-D model shown in Fig. 11 from the observed gravity field in Fig. 5. Contours are in milligals.

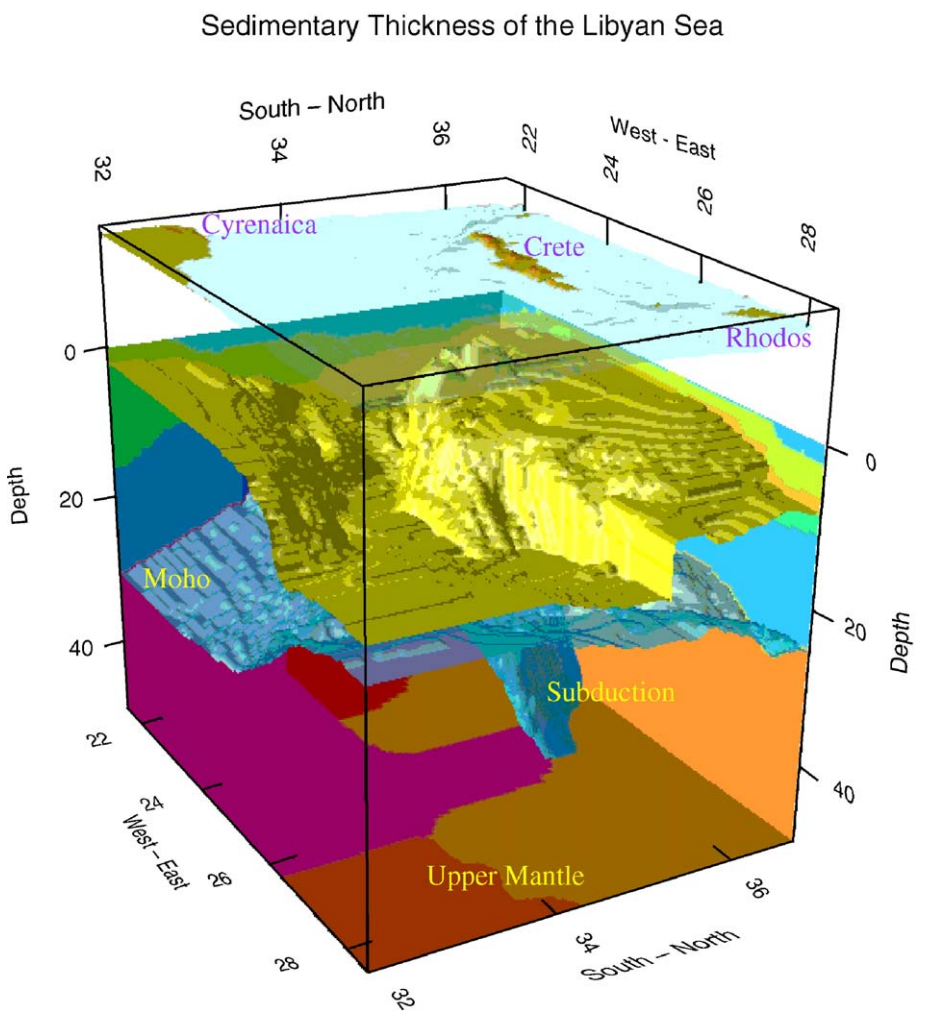

Fig. 13. A 3-D density model developed by 3-D gravity modelling for the East Mediterranean Ridge between the Cretan Sea and Cyrenaica. View from southeast: the upper surface shows the base of sediments between the two continental plates of Africa and the Aegean microplate, separated by the oceanic crust of the Eastern Mediterranean Ridge. More than 15 km thick sediments are deposited on the oceanic part of the model. Upper mantle of different density is shown by different colors in the lower part of the figure. (For interpretation of the references to colour in this figure legend, the reader is referred to the web version of this article.)

depends on the geometry of the continental margin of the Aegean microplate.

The crust–mantle boundary presented in Fig. 8 shows the deep deformation of the crust and upper mantle due to the present active subduction. The transition of the 32 to 34 km thick crust of Central Crete to the thinner one of Eastern Crete (24 to 26 km) is accomplished along a NW–SE oriented zone. The oceanic lithosphere below Crete is separated from the overlying continental crust along this NW–SE orientated front. This is also the limit of the low density mantle of the South Aegean volcanic arc to that of high density below the Libyan and Ionian Seas. The subducted slab plunges steeply under the eastern Cretan Sea and its geometry is defined by the high seismicity of the Wadati–Benioff zone (Galanopoulos, 1973; Makropoulos, 1984; Papazachos and Papazachos, 1997) that can be followed below the volcanoes of the central and eastern Aegean Sea. This is also seen in Fig. 14 where the 3-D picture of the Moho is presented. At the area of the Dodecanese, approximately 250 km to the northeast, the volcanic belt of Cos–Nisyros indicates that the subducted slab from western Crete has reached the correct depth for mobilization of the magma that triggers the andesitic volcanism of the southeastern Aegean Sea (Fytikas et al., 1984). The orientation of the subducted slab shows that the present active subduction is northeast–southwest oriented, de-

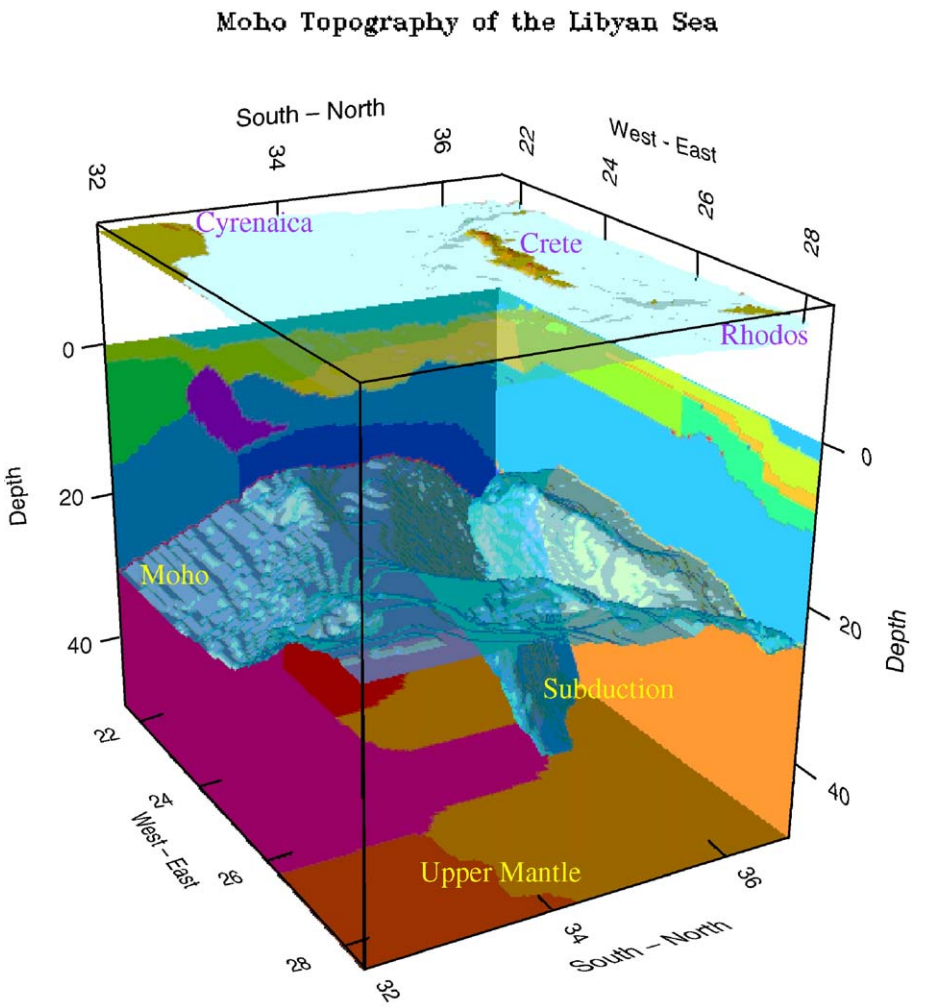

Fig. 14. The 3-D model of the Moho topography of the Eastern Mediterranean Ridge between the Cretan Sea and Cyrenaica. View from southeast: this is obtained from the 3-D model of Fig. 13 by stripping off the sediments. Upper mantle of different density is shown by different colors in the lower part of the figure.

fining the present relative motion between Europe and Africa.

6. Discussion and conclusions

The five seismic lines recently recorded along the Cretan and Libyan Seas (Makris and Broenner, 2001; Bohnhoff et al., 2001; Broenner, 2003), together with the seismic results from the ESPs (two-ship seismic experiment) published by De Voogd et al. (1992), Fruehn et al. (2002) and Jones et al. (2002), provided for the first time velocity models and the structure of the deep basins and crust at the collision front between the Aegean microplate to the north and the oceanic lithosphere to the south and west of Greece. For the first time we see the limits of the crustal types and the structure of their margins. Three-dimensional gravity modelling permitted to extend the seismic 2-D results in 3-D density models for the entire area between the Cretan Sea and Libya. It is now obvious that the backstop of the sediments west and south of Crete is defined by the continent–ocean transition of the crust and lithosphere and that two distinctly different types of margins in the Libyan Sea are distinguished. The Aegean microplate side is steep, defining the edge of a deep depot of sediments that exceed 13 to 14 km in thickness. They rest on oceanic lithosphere, actively subducting in a northeastern direction below the Aegean microplate. In doing so, parts of these sediments can follow the oceanic lithosphere below the Cretan Sea and transport water together with the oceanic crust at depth. This serpentinizes the oceanic lithosphere and

at the appropriate pressure and temperature mobilizes the andesitic magma causing the Aegean volcanism. Thus, the density distribution is disturbed, triggering isostatic rebalancing and uplift of hot, less dense magma, below the Cretan Sea. The isotherms are elevated by convection (Makris and Stobbe, 1984) and observed on the surface heat flow permit to reconstruct the temperature distribution below the Cretan Sea and the Mediterranean Ridge (Jongsma, 1974; Makris, 1977; Cermak, 1979; Makris and Stobbe, 1984; Fytikas et al., 1984). In contrast to the Cretan Sea, the external parts of the Hellenic Arc have cold dense lithosphere, as confirmed by high P_n-values of the seismic waves (8.0 km/s) and density (up to 3.33×10^3 kg/m^3) (see also Makris, 1977; Makris and Stobbe, 1984; De Voogd et al., 1992; Truffert et al., 1993). The African Libyan margin is significantly stretched, compared to the African craton, before it gradually sinks to depth of 15 km underlying the oceanic basin, as seen in Fig. 7 and also in the 3-D presentation of the sediments in Fig. 13. The huge ramp of stretched continental crust to both sides of the MR sedimentary basins of the oceanic domain between Africa and Europe accommodate thick sedimentary series partly deposited and partly obducted in the subsiding domain. Magnetic and gravity anomalies indicate that ophiolites are participating in this process to the south, along the North African margin (see also Makris and Wang, 1994). The limits of the internal and external parts of the Mediterranean Ridge, defined by Chaumillon and Mascle (1997), Mascle et al. (1999) and by Huguen et al. (2001), coincide with the edge of the African continental ramp in the south and with the fringes of the Aegean continental microplate south of Crete. They define areas of different styles of deformation: the one controlled by subduction to the NNE and the other by obduction to the south. The geometry of the Aegean microplate to the west, southwest of Crete and its connection to the Pliny and Strabo trenches, south of Crete, suggests that strike-slip motion exists along both these fault systems. An independent 3-D interpretation of the gravity field (Casten and Snopek, 2006) shows some differences to our density model. We disagree on: (1) the crustal thickness at the western part of Crete and (2) the subduction geometry of the slab below Crete. We have strictly constrained our model by the seismic results on Crete and the Cretan Sea. These data define the crustal thickness below western Crete to 32 km, including the oceanic slab, and also shows that the subduction is northeast orientated. The oceanic slab is decoupled from the continental crust along a northwest southeast striking front in the Cretan Sea and central Crete. The deep seismicity and seismically obtained crust and geometry of the subducting slab constrain the density model and its interpretation as presented above.

Acknowledgments

We thank the two reviewers who read the manuscript critically and helped us improve the final version. The evaluation and modelling was financially supported by GeoPro Hamburg.

References

Birch, F., 1960. The velocity of compressional waves in rocks to 10 kilobars (Pt. 1). J. Geophys. Res. 4, 1083–1102.

Birch, F., 1961. The velocity of compressional waves in rocks to 10 kilobars (Pt. 2). J. Geophys. Res. 66 (7), 2199–2224.

Brennecker, J., Lelgemann, D., Reinhart, E., Torge, W., Weber, G., Wenzel, H., 1983. A European astrogravimetric geoid. Dtsch. Geod. Komm. (B. Angew. Geodäs.) 269, 1–115.

Broenner, M., 2003: Untersuchung des Krustenaufbaus entlang des Mediterranen Rückens abgeleitet aus geophysikalischen Messungen. Ph.D. Dissertation, Universität Hamburg: 1–170.

Bohnhoff, M., Makris, J., Papanikolau, D., Stavrakakis, G., 2001. Crustal investigation of the Hellenic subduction zone using wide aperture seismic data. Tectonophysics 343, 239–262.

Casten, U. and Snopek, K., 2006. Gravity modelling of the Hellenic subduction zone—a regional study, Tectonophysics 417, 183–200.

Cermak, V., 1979. Heat flow map of Europe. In: Cernak, V., Rybach, L. (Eds.), Terrestrial Heat Flow in Europe, pp. 3–40.

Cermak, V., Hurtig, E., Kutas, R.I., Lubimova, E.A., Mongelli, F., Morgan, P., Smirnov, Y.B., Tescan, A.K., 1977. Heat flow map of southern Europe and the Mediterranean region. Proc. Int. Congr. Therm. Waters, Geothrm. Energy 1, 149–168.

Chapin, D., 1998. Gravity instruments: past, present, future. Lead. Edge 17, 100–112.

Chaumillon, E., Mascle, J., 1997. From foreland to forearc domains: new multichannel seismic reflection survey of the Mediterranean ridge accretionary complex (Eastern Mediterranean). Mar. Geol. 138, 237–259.

Chaumillon, E., Mascle, J., Hoffmann, J., 1996. Deformation of the western Mediterranean Ridge: importance of Messinian evaporitic formations. Tectonophysics 263, 163–190.

Department of Geodesy and Geophysics, 1975. Geophysical Data Report of the Eastern Mediterranean Sea. Cambridge University, Cambridge, England.

De Voogd, B., Truffert, C., Chamot-Rooke, N., Huchon, P., Lallemant, S., Le Pichon, X., 1992. Two-ship seismic soundings in the basins of the Eastern Mediterranean Sea (Pasiphae Cruise). Geophys. J. Int. 109, 536–552.

Fruehn, J., Reston, T., von Huene, R., Bialas, J., 2002. Structure of the Mediterranean Ridge accretionary complex from seismic velocity information. Mar. Geol. 186, 43–58.

Fytikas, M., Innocenti, P., Manetti, P., Mazzuoli, R., Peccerillo, A., Villari, L., 1984. Tertiary to Quaternary evolution of the volcanism in the Aegean region. In: Dixon, J.E., Robertson (Eds.), The Geological Evolution of the Eastern Mediterranean, Geol. Soc. Special Publ., vol. 17, pp. 687–700.

Galanopoulos, A., 1973. Plate tectonics in the area of Greece as reflected in the deep focus seismicity. Ann. Geofis. 26, 85–105.

Hartmann, J.M., 1995. Geophysikalische Untersuchungen in der Ionischen See. Berichte aus dem ZMK, Reihe C, Nr. 10, Universitat Hamburg.

Hartung, M., 1987. Geophysikalische Vermessung des Kreta-Meeres unter besonderer Berücksichtung refractionsseismischer Daten; Diplomarbeit, Universität Hamburg.

Hirschleber, H.B., Hartmann, J.M., Hieke, W., 1994. The Mediterranean Ridge accretionary complex and its forelands—seismic reflection studies in the Ionian Sea. In: Ansorge, R. (Ed.), Schlaglichter der Forschung zum 7. Jahrestag Universitat Hamburg 1994, Hamburger Beitr. Wissenschaftsgeschichte, vol. 15, pp. 491–509.

Huguen, C., Mascle, J., Chaumillion, E., Woodside, J.M., Benkhelil, J., Kopf, A., Volkonskaya, A., 2001. Deformation styles of the eastern Mediterranean Ridge and surroundings from combined swath mapping and seismic reflection profiling. Tectonophysics 343, 21–47.

Jolivet, L., Brun, J.P., Gautier, P., Lallemand, S., Patriat, M., 1994. 3-D kinematics of extension in the Aegean from the early Miocene to the present, insights from the ductile crust. Bull. Soc. Geol. Fr. 165, 195–209.

Jones, K.A., Warner, M., Le Meur, D., Pascal, G., Tay, P.L., the IMERSE Working Group, 2002. Wide-angle images of the Mediterranean Ridge backstop structure. Mar. Geol. 186, 145–166.

Jongsma, D., 1974. Heat flow in the Aegean Sea. J. R. Astron. Soc. 37, 337–346.

Kahle, H.-G., Straub, C., Reilinger, R., McClusky, S., King, R., Hurst, K., Veis, G., Kastens, K., Cross, P., 1998. The strain rate field in the eastern Mediterranean region, estimated by repeated GPS measurements. Tectonophysics 294, 237–252.

Kastens, K., 1991. Rate of outward growth of the Mediterranean ridge accretionary complex. Tectonophysics 199, 25–50.

Le Pichon, X., Angelier, J., 1979. The Hellenic Arc and Trench system: a key to the neotectonic evolution of the Eastern Mediterranean. Tectonophysics 60, 1–42.

Le Pichon, X., Chamot-Rooke, N., Lallemant, S., 1995. Geodetic determination of the kinematics of central Greece with respect to Europe; implications for Eastern Mediterranean Tectonics. J. Geophys. Res. 100, 12675–12690.

Makris, J., 1977. Geophysical investigations in the Hellenides. Hamburg Geophys. Einzelschr 34 (1) (124 pp.).

Makris, J., 1978. The crust and upper mantle of the Aegean region from deep seismic soundings. Tectonophysics 46, 269–284.

Makris, J., Broenner, M., 2001. Crustal shortening along the Cretan Arc obtained by active seismic experiments. Report du 36-e Congres de la Commission Internationale pour L'Exploration Scientifique de la mer Mediterranee, CIESM Congress Proceedings, vol. 36. Monte-Carlo, Monako.

Makris, J., Morelli, C., 1994. The Bouguer gravity map of the Mediterranean Sea (IBCM-G). In: Hall, J.K. (Ed.), IBMCM-supporting volume—Chapter 28. Interngovernmental Oceanographic Commission of UNESCO, Jerusalem.

Makris, J., Morelli, C., Zanolla, C., 1998. The Bouguer gravity map of the Mediterranean Sea (IBCM-G). Boll. Geofis. Teor. Appl. 39 (2), 79–98.

Makris, J., Stobbe, C., 1984. Physical properties and state of the crust and upper mantle of the Eastern Mediterranean Sea deduced from geophysical data. Mar. Geol. 55, 347–363.

Makris, J., Vees, R., 1977. Crustal structure of the Aegean Sea and the Islands Evia, Crete, Greece, obtained by refraction seismic experiments. J. Geophys. 42, 329–341.

Makris, J., Wang, J., 1994. Bouguer gravity anomalies of the Eastern Mediterranean Sea. In: Krasheninnikov, V. (Ed.), Special Publication of the Geological Survey of Israel. John K. Hall, Jerusalem.

Makropoulos, K., 1984. Greek tectonics and seismicity. Tectonophysics 106, 275–304.

Mascle, J., Huguen, C., Benkhelil, J., Chamot-Rooke, N., Chaumillion, E., Foucher, J.P., Griboubard, R., Kopf, A., Lamarche, G., Volkonskaia, A., Woodsite, J., Zitter, T., 1999. Images may show start of European–African collision. Eos, Transactions, AGU, v.80, no. 37, pp. 421, 425, 428.

McClusky, S., Balassanian, S., Barka, A., Demir, C., Ergintav, S., Georgiev, I., Gurkan, O., Hamburger, M., Hurst, K., Kahle, H., Kastens, K., Kekelidze, G., King, R., Kotzev, V., Lenk, O., Mahmoud, S., Mishin, A., Nadariya, M., Ouzounis, A., Paradissis, D., Peter, Y., Prilepin, M., Reillinger, R., Sanli, I., Seeger, H., Tealeb, A., Toksőz, M.N., Veis, G., 2000. Global positioning system constraints on plate kinematics and dynamics in the eastern Mediterranean and Caucasus. J.Geophys. Res. 105 (B3), 5695–5719.

McKenzie, D.P., 1978. Active tectonics of the Alpine–Himalaya belt: the Aegean Sea and surrounding regions. Geophys. J. R. Astron. Soc. 55, 217–254.

Morelli, C., Val'chuk, S., 1988. The International Bathymetry Chart of the Mediterranean (I.B.C.M.) published under authority of the Intergovernmental Oceanographic Commission of UNESCO in J.K. Hall et al., supporting volume, Jerusalem, Israel, 10p.

Morelli, C., Pisani, M., Gantar, C., 1965. Geophysical studies in the Aegean Sea and in the Eastern Mediterranean. Boll. Geofis. XVIII (66).

Nafe, J.E., Drake, Ch.L., 1963. Physical properties of marine sediments. The Sea, Interscience, vol. 3.

Papazachos, C., Nolet, G., 1997. *P* and *S* deep velocity structure of the Hellenic area obtained by robust nonlinear inversion of travel times. J. Geophys. Res. 102, 8349–8367.

Papazachos, V., Papazachos, C., 1997. In: Ziti (Ed.), The Earthquakes of Greece, pp. 1–304.

Polonia, A., Camerlenghi, A., Davey, F., Storti, F., 2002. Accretion, structural style and syn-contractional sedimentation in the Eastern Mediterranean Sea. Mar. Geol. 186, 127–144.

Pondrelli, S., Morelli, A., Ekström, G., Boshi, E., Dziewonski, A.M., 2002. European–Mediterranean regional centroid–moment–tensors: 1997–2000. Phys. Earth Planet. Inter. 130, 71–101.

Reillinger, R.E., McClusty, S.C., Oral, M.B., King, R.W., Toksoz, M.N., 1997. Global Positioning System measurements of present day crustal movements in the Arabia–Africa–Eurasia plate collisional zone. J. Geophys. Res. 102, 9983–9999.

Reston, T.J., Fruehn, J., von Huene, R., IMERSE Working Group, 2002. The structure and evolution of the western Mediterranean Ridge. Mar. Geol. 186, 83–110.

Sandwell, W.H.F., Smith, D.T., 1997. Marine gravity anomaly from Geosat and ERS-1 satellite altimetry. J. Geophys. Res. 102, 10039–10054.

Spakman, W., Wortel, M.J.R., Vlaar, N.J., 1988. The Hellenic subduction zone: a tomographic image and its geodynamic implications. Geophys. Res. Lett. 15 (1), 60–63.

Talwani, M., Lamar, W., 1959. Rapid gravity calculation for two-dimensional bodies with applications to the Mendicino Submarine Fracture Zone. J. Geophy. Res. 64 (1), 49–59.

Tchernychev, M., Makris, J., 1996. Fast calculations of gravity and magnetic anomalies based on 2-D and 3-D grid approach. SEG 66nd Ann. Internat. Mtd., pp. 1136–1138.

Truffert, C., Chamot-Rooke, N., Lallemant, S., De Voogd, B., Huchon, P., Le Pichon, X., 1993. The crust of the Western Mediterranean Ridge from deep seismic data and gravity modelling. Geophys. J. Int. 114, 360–372.

Tsokas, G., Hansen, R., 1997. Study of the crustal thickness and the subducting lithosphere in Greece from gravity data. J. Geophys. Res. 102, 20585–20597.

Wessel, P., Smith, W.H.F., 1998. New, improved version of Generic Mapping Tools released. Eos Trans., AGU 79, 579.